U. of Iowa 93-19

A Study of Saturn's E-Ring Particles Using the Voyager 1 Plasma Wave Instrument

by

D. Tsintikidis[1], W. S. Kurth[1],

D. A. Gurnett[1], and D. D. Barbosa[2]

September 1993

[1]Dept. of Physics and Astronomy, The University of Iowa, Iowa City, IA 52242

[2]Institute of Geophysics and Planetary Physics, University of California, Los Angeles, CA 90024

ABSTRACT

The flyby of Voyager 1 at Saturn resulted in the detection of a large variety of plasma waves, e.g., chorus, hiss, and electron cyclotron harmonics. Just before the outbound equator crossing, at about 6.1 R_S, the Voyager 1 plasma wave instrument detected a strong, well-defined low-frequency enhancement. Initially it was suggested that plasma waves might be responsible for the spectral feature but more recently dust was suggested as at least a partial contributor to the enhancement. In this report we present evidence which supports the conclusion that dust contributes to the low-frequency enhancement. A new method has been used to derive the dust impact rate. The method relies mainly on the 16-channel spectrum analyzer data. The few wideband waveform observations available (which have been used to study dust impacts during the Voyager 2 ring plane crossing) were useful for calibrating the impact rate from the spectrum analyzer data. The mass and, hence, the size of the dust particles were also obtained by analyzing the response of the plasma wave spectrum analyzer. The results show that the region sampled by Voyager 1 is populated by dust particles that have rms masses of up to few times 10^{-11} g and sizes of up to a few microns. The dust particle number density is on the order of 10^{-3} m^{-3}. The optical depth of the region sampled by the spacecraft is 1.04 x 10^{-6}. The particle population is centered about 2500 km south of the equatorial plane and has a north-south thickness of about 4000 km. Possible sources of these particles are the moons Enceladus and Tethys whose orbits lie within the E-ring radial extent. These results are in reasonable agreement with photometric studies and numerical simulations.

1. INTRODUCTION

The dust environment of Saturn has been studied extensively. A great deal of knowledge has resulted from studying the direct detection of dust, i.e., from the micrometeoroid bombardment detectors ("beer can" experiment) onboard Pioneer 11 [Humes, 1980], and from the plasma wave and planetary radio astronomy instruments onboard Voyager 2 [Scarf et al., 1982; Warwick et al., 1982]. The dust dynamics have also been (and are still being) studied using analytical and numerical techniques, e.g., Xu and Hupis [1985], Burns and Schaffer [1989], Horanyi et al. [1992]. During the Voyager 2 planetary encounters, the plasma wave instrument detected regions of intense, impulsive noise at each of the three outer planets (Saturn, Uranus, Neptune) that have been attributed to micron-sized dust particles hitting the spacecraft body [Gurnett et al., 1983, 1987, 1991; Aubier et al., 1983; Pedersen et al., 1991; Tsintikidis et al., 1993]. As a particle hits the spacecraft at a relative velocity of up to a few tens of kilometers per second, it is vaporized. A small, partially ionized cloud of gas is produced and expands radially outward from the impact site. Part of the charge in the cloud is collected by the electric antennas onboard the spacecraft. The mass and the size of the particles can be estimated by analyzing the amplitude of the voltage pulse as it is recorded by the 16-channel spectrum analyzer (low resolution data). Also, the wideband waveform receiver data frames (high resolution data) can be used to calculate the impact rate. When the impact rate is combined with the spacecraft cross-sectional area and the relative velocity between the spacecraft and the dust particles, the particle number density can also be calculated. Eventually a picture

of the dust environment can be created in the region sampled by the spacecraft (see, for example, Figure 13 of Gurnett et al. [1991]).

A fortunate event during the Voyager 2 encounters with the three outer planets was the fact that the plasma wave instrument recorded wideband data within and on either side of the dust rings. However, during the Voyager 1 flyby of Saturn the relatively few wideband frames that were recorded were located well out of the equatorial plane. Hence, the derivation of the impact rate profile (and consequently the number density profile) as was done by Tsintikidis et al. [1993] was not possible. To overcome this deficiency we have developed a new method of determining the impact rates by using the 16-channel spectrum analyzer data and the few high resolution data frames that are available to calibrate the new method.

In this paper we present a detailed study of the low resolution data recorded by the plasma wave instrument onboard Voyager 1 around the time of closest approach to Saturn. We give: (1) a detailed description of the data used in the study, (2) a thorough description of the method used to derive our results, (3) an interpretation of the data in terms of number density, mass and sizes of the dust particles, (4) a validation of our results compared with theoretical predictions and results from other independent photometric studies, and (5) a short discussion of the origin of the particles.

2. OBSERVATIONS

A summary of the observations of Voyager 1 at Saturn can be seen in Plate 3 of Kurth and Gurnett [1991]. Among other features there is one tentatively labeled dust impacts centered around 0410 spacecraft event time (SCET) on November 13, 1980. At that time the spacecraft was outbound at approximately 6 R_S (1 R_S = 60,330 km), just below the equatorial plane. The feature looks similar to the intense, impulsive, dust-attributed noise that has been observed during the other planetary encounters accomplished by Voyager 2 (see the dust signatures at Uranus and Neptune in Plates 4 and 5 of Kurth and Gurnett [1991]). However, the most definitive proof that dust exists in the area sampled by the spacecraft comes from the waveform data. The waveform signature of a dust impact consists of a single pulse and is unlike any known plasma wave waveform. The waveform data can also be used to determine particle impact rates and number densities simply by following the technique of Gurnett et al. [1987, 1991], or Tsintikidis et al. [1993]. However, no wideband waveform frames (high resolution data) were available at the time that Voyager 1 crossed the equatorial plane of Saturn. Hence, it was not clear if the feature was a result of plasma wave activity or dust impacts or both. Barbosa and Kurth [1993] interpreted the Voyager 1 plasma wave observations at Saturn's inner magnetosphere in terms of whistler mode and electrostatic electron cyclotron harmonic waves. These conclusions were reached when the authors theoretically calculated the critical flux of the superthermal electrons that can produce whistler-mode waves and electron cyclotron harmonic waves through a loss-cone instability. Furthermore, they concluded that a moderate anisotropy in the hot electron population exists in the equatorial region at L values ranging from 5 to 8.

However, Barbosa and Kurth [1993] did not exclude the possibility that some of this noise may be caused by dust impacts. In addition, Kurth and Gurnett [1991] also suggested that a low frequency enhancement, below the electron cyclotron frequency, could be attributed to dust impacts, especially near the ring plane crossing, from about 0400 to 0425 SCET. The purpose of the present study is to determine what portion of the enhancement in question can be attributed to dust impacts.

The antennas used by the Voyager plasma wave receiver are operated as an electric dipole, meaning that the plasma wave instrument measures the potential difference between the two antenna elements. The signals from the antennas are processed in two ways. First, a 16-channel spectrum analyzer provides absolute measurements of the voltage spectral densities covering the range from 10 Hz to 56 kHz. There are 4 channels per decade spaced logarithmically (e.g., 10.0, 17.8, 31.1, 56.2 Hz). The spectrum analyzer has two logarithmic compressors. Each logarithmic compressor consists of a detector whose output is a voltage that is proportional to the logarithm of the signal amplitude passing through the channel that is currently being sampled. The 16-channel spectrum analyzer does not have peak detection. The analyzer is a step frequency receiver which means that one channel after another is sampled until the full spectrum has been obtained. Actually the lower and upper 8 channels are processed separately by the two logarithmic compressors and the two frequency ranges are stepped through nearly simultaneously. The filters have bandwidths of $\sim \pm$ 15% for the lowest 8 frequencies and $\sim \pm 7.5\%$ for the highest 8 frequencies. The time constant of the logarithmic compressor is about 50 ms for the lower 8 channels and about 42 ms for the upper 8 channels [Kurth et al., 1983]. A full 16-channel spectral scan is completed once every 4 s. Second, a wideband receiver provides waveforms in a frequency band from 50 Hz to 12 kHz. The wideband data

are obtained in "frames" that are 48-s long. Each frame contains 800 60-ms subsequences consisting of 4-bit measurements of the potential between the two antenna elements sampled at a rate of 28,800 s^{-1}. An automatic gain control (AGC) is used to maintain an almost constant output signal amplitude to provide a large dynamic range. The time constant of the AGC is 0.5 s. The PWS instrument onboard Voyager 1 is identical to the instrument onboard Voyager 2. For more details on the instrumentation see Scarf and Gurnett [1977].

Figure 1 shows the Voyager 1 trajectory by Saturn projected onto a meridional plane through the spacecraft. The spacecraft went as close as 3.05 R_S at -39.51 degrees latitude on November 12. On the outbound leg it crossed the equatorial plane at 0418:30 SCET on November 13, 1980 at 6.24 R_S. Figure 2 shows all the channels of the 16-channel spectrum analyzer for a 4-hour period centered on the equatorial plane crossing. A relatively long smooth, background can be seen for about half an hour centered at approximately 0410 SCET, with a series of bursty signals superimposed on the background. There are certain similarities between the spectrum obtained at Saturn by the Voyager 1 PWS and the spectra obtained at Saturn, Uranus, and Neptune by the Voyager 2 PWS [Tsintikidis et al. 1993, Gurnett et al., 1987, 1991]. The similarities are the spiky nature of the signals, the gradual increase and decrease in the intensity (even though the change is slow and the intensity does not reach a very distinct maximum for the case of Voyager 1 at Saturn). The fact that the intensity decreases with increasing frequency and drops to the instrument noise level at higher frequencies (above a few kHz) is also consistent with what has been recorded by the Voyager 1 and 2 PWS instrument in the various planetary encounters. We attribute the bursty signals to dust impacts.

A grey-scale spectrogram of the 16-channel spectrum analyzer data taken over a longer period of time is shown in Figure 3. In the figure, black is the most intense and white is the

least intense plasma wave activity. The most intense feature ranges in frequency from 10 Hz to 1 kHz, starting slightly before 0400 SCET, and lasts for about 25 minutes. From now on, we will refer to this feature as the low-frequency equatorial enhancement. The duration of the enhancement above the lower hybrid frequency f_{LHR} is somewhat longer than at lower frequencies. The lower hybrid resonance frequency is defined as $f_{LHR} = \sqrt{f_{ce}f_{ci}}$, where f_{ce} is the electron gyrofrequency and f_{ci} is the proton cyclotron frequency. As mentioned by Barbosa and Kurth [1993] the low-frequency equatorial enhancement exists over the entire region below the electron cyclotron frequency, which makes these waves good candidates for whistler-mode noise since whistler mode emissions propagate below the electron cyclotron frequency. We inspected plasma wave spectra obtained at Earth with the Galileo plasma wave instrument and a number of other missions. Typically, the whistler mode intensity decreases substantially below the lower hybrid resonance frequency, f_{LHR} (see line profile in Figure 3). It should be mentioned that the region sampled by the Voyager 1 PWS instrument consists of protons but is probably dominated by a heavier species that could possibly be O^+ or N^+ [Bridge et al., 1981]. If, for example, the plasma consists of 80% O^+ and 20% protons then the lower hybrid resonance frequency is reduced by a factor of 2 below the profile provided in Figure 3. Hence, minimal plasma wave contamination would be expected in the lowest three channels.

Clearly the enhancement is not as sharply peaked as dust impacts observed at other planetary encounters (see the features labeled dust in Plates 4 and 5 of Kurth and Gurnett [1991]). The rapid peak in intensity and the clear definition of similar enhancements that Voyager 2 recorded in Saturn, Uranus, and Neptune were indications that the noise was due to dust. The primary difference between the Voyager 1 equatorial enhancement and the dust

signatures observed by Voyager 2 at Saturn, Uranus, and Neptune are that the Voyager 1 signature is less intense and more broadly distributed in time.

Gurnett et al. [1983] studied a large number of wideband data frames as they were recorded by both Voyager spacecraft (see their Table 1 and 2). Their results indicate the presence of dust throughout the Saturnian system. In addition, we know that Voyager 1 crossed the diffuse E-ring. One can also look at the limited number of the Voyager 1 wideband receiver data frames, recorded before the equatorial plane crossing, to be further convinced that there is dust throughout the Saturn system. At the time the last frame was taken at 0326 SCET on November 13, 1980, before the equator crossing (position A in Figure 1), Voyager 1 was at a radial distance of 5.38 R_S and latitude of -4.53 degrees. A representative sample of dust impact signatures can be seen in Figure 4. Clearly they have characteristics identical to the wideband waveforms observed in the other planetary encounters of Voyager 2. Since these waveforms have been repeatedly studied (i.e., Gurnett et al. [1983, 1987, 1991]; Tsintikidis et al. [1993]), we are not going to describe them further. Waveforms similar to Figure 4 have also been observed during the other times that wideband data were available (the day of the year and the times are shown in the first and second columns respectively of Table 1) during the Voyager 1 encounter with Saturn. For a complete summary of the Voyager 1 wideband impulse rates see Table 1 of Gurnett et al. [1983]. The frames will be useful later on in calibrating the impact rates as they are derived from the 16-channel spectrum analyzer.

Further support for the fact that dust exists in the regions traversed by the Voyager 1 spacecraft can be found in Figure 5. This figure shows a 1-min average spectrum from 0413 to 0414 SCET, chosen during the time when the low-frequency equatorial enhancement is most prominent. Other 1-min intervals give similar spectra. The spectrum varies approximately as

f^{-4} which is in agreement with the spectra obtained by the Voyager 2 planetary radio astronomy instrument at Saturn [Aubier et al., 1983] and Uranus [Meyer-Vernet et al., 1986] and to the spectra obtained by the Voyager 2 plasma wave instrument at Saturn [Tsintikidis et al., 1993] and Neptune [Gurnett et al., 1991]. The f^{-4} behavior of the spectral density agrees with the theoretically calculated spectral density if the signal is attributed to dust impacts as was shown by Meyer-Vernet et al. [1986]. Because of the plasma wave activity occurring at the same time, one should not expect strict agreement with a f^{-4} spectrum. The existence of dust impacts in the high resolution data, the fact that the spacecraft traversed a tenuous ring, and the shape of the spectrum from the low resolution data all lead us to the conclusion that the Voyager 1 PWS instrument is responding to dust impacts as it crossed the E ring near 0410 SCET.

3. BRIEF REVIEW OF THE COUPLING MECHANISM

When a small particle hits a solid surface at a high velocity, i.e., a few kilometers per second or greater, the particle and some of the surface material is instantly vaporized and heated to a high temperature $\sim 10^5$ °K [Gurnett et al., 1991]. At these high temperatures, a portion of the gas is ionized, thereby producing a small plasma cloud that expands radially outward from the impact site. Results of laboratory experiments, [Grün, 1981] show that the charge Q released at the impact site is proportional to the mass m of the impacting particle,

$$Q = k\ m \tag{1}$$

where k is a yield constant that depends on the velocity of the particle and the composition of the particle and the target. The yield constant varies approximately as the cube of the speed [Grün, 1981]. During the time interval that the low-frequency equatorial enhancement was recorded, the relative speed between the spacecraft and particles in prograde, circular orbits was very high, approximately 29.3 km/s. At this speed, which is approximately constant during the time of interest, the yield constant is ~ 2.05 C/g.

The basic assumption in our study is that only a fraction α of the charge released after the impact is collected by the antennas, hence, producing a voltage pulse of amplitude:

$$V = \alpha \frac{Q}{C_A} \tag{2}$$

where C_A is the antenna capacity. The constant α is the charge collection coefficient. The coefficient is dimensionless and was estimated by Tsintikidis et al. [1993] to be 0.0078. The new value was calculated by using the Voyager 2 PRA spectra to calibrate the PWS spectra

obtained at all available ring plane crossings, namely at Saturn, Uranus, and Neptune (both inbound and outbound for the latter). It was discussed that the low-frequency equatorial enhancement recorded by the Voyager 1 PWS during the ring plane crossing of Saturn cannot be attributed exclusively to dust impacts. Hence, the comparison of the PWS and PRA spectra cannot be used in this case in order to derive α. For this reason the average value of α was used instead. The collection coefficient estimate is considered to be better than previous calculations because it is an average value of the different collection coefficients calculated for each planetary encounter. The value of α differs from the value calculated by Gurnett et al. [1987] by a factor of almost 2. The collection coefficient is still of the same order of magnitude for each ring plane crossing. The implicit assumption is that the same value of α that was calculated based on Voyager 2 data can be used for Voyager 1 since both spacecraft have identical PWS and PRA instruments. For more details on the evaluation of α, see Tsintikidis et al. [1993].

4. IMPACT RATES AND PARTICLE NUMBER DENSITIES

Next, we estimate the impact rate and the number density of the impacting particles. The number density, n, is given by

$$R = n\ U\ A_{sc} \tag{3}$$

where R is the impact rate, U is the relative speed between the spacecraft and the particles and A_{SC} is the effective area of the spacecraft body. As discussed earlier the relative speed between the spacecraft and particles in a circular, prograde, equatorial orbits is 29.3 km/s. The effective area is 1.66 m^2 as computed by Gurnett et al. [1983]. The greatest difficulty in computing the number density lies in calculating the impact rate, R. The 16-channel spectrum analyzer data, since it was the only data set available around the time of the equatorial plane crossing, must be used to derive impact rates.

We considered only the lowest 8 channels to look for impacts since no bursty signals can be seen in the higher channels. Figure 6 shows the lower 8 channels of the spectrum analyzer. The figure concentrates on the time that the low-frequency equatorial enhancement was most prominent. The smooth background and the bursty signals are more easily seen now. Figure 6 was divided into one-minute intervals from 0400 to 0425 SCET. Each burst exceeding a preset threshold intensity of 7.07×10^{-4} V (indicated by the arrows in Figure 6) is attributed to a dust impact. The criterion for choosing the threshold as 7.07×10^{-4} V was to make sure that the bursts were clearly above the smooth background. As was mentioned before the

16-channel spectrum analyzer is a step frequency receiver. The stepping scheme precludes the possibility simultaneous samples.

Another consideration included in the analysis was the duty cycle of the spectrum analyzer. The instrument spends 0.05 seconds at each channel times 8 channels (or 0.4 seconds) during a total of 4 seconds available for an entire spectral sweep. Hence, the duty cycle was 0.10.

An additional uncertainty involved is that of the number of impacts associated with each peak. The typical time scale of a dust impact as recorded by the wideband receiver is about 10 ms [Gurnett et al., 1983; Tsintikidis et al., 1993]. Each point plotted in Figure 6 represents a $\sim$50 ms measurement period during which any number of dust impacts may have occurred. However, using the maximum impact rate derived from the wideband observations (e.g., $\sim$ 16 s^{-1} at 0326 SCET) it is apparent that, on average, there is only about one impact per measuring period. If the rates are more than 20 s^{-1}, then it is increasingly likely that 2 or more impacts would occur within a 50-ms interval, and our assumption of 1 impact per peak becomes a lower limit. There is no way of telling the number of impacts solely from the spectrum analyzer data. Throughout this study it will be assumed that each burst corresponds to a single dust impact. This assumption is going to be further justified shortly.

After each planetary encounter the spectrum analyzer data are processed in order to remove unwanted data in the following sense: bursty signals that are clearly due to instrument interference (e.g., due to the Low Energy Charged Particles instrument's stepper motor) because of their periodic nature are removed from the data set. This is indicated by the periodic gaps in Figure 6. Hence, the contribution of the aforementioned interference is close to zero for the signal under study. However, some unpredictable spacecraft-related interference signals do still

occur. The primary source of these unpredictable interference signals in the lower 8 channels is due to random thruster firings. There is no data from the spacecraft that indicate exactly when the thruster firings occur. However, it is necessary to correct the impact rates by taking the contribution of the thruster activity into account.

To correct for thruster interference effects various times were considered during which the spacecraft was far from the planet (out in the solar wind) where actual dust impacts are highly unlikely. Outside of the Saturnian system, it can be assumed that the only significant source of low-frequency bursts is thruster activity. For these periods, we calculated the spurious event rates exceeding our threshold, and corrected for the duty cycle. The results can be seen in Table 2. The average spurious event rate was found to be 0.08 s^{-1} and it was subtracted from the impact rate determined closer to the planet (column 4 in Table 1).

While the spacecraft was close to the planet and before it crossed the equatorial plane, there were six times during which 48-sec wideband waveform data frames were taken. At these six times the impact rates were found by visually inspecting the data frames (column 5 in Table 1). The highest impact rate occurred at 0326 SCET and was 15.87 s^{-1}. The probability of having a second impact during a 50-ms measurement is 0.6% which is a very low value. Hence, the assumption that there is only one impact per 50-ms peak is justified for most measurement periods. There is a slight difference between the newly derived impact rates and the ones listed in Table 1 of Gurnett et al. [1983]. In general, the new impact rates have higher values than the older ones. The difference is attributed to the fact that in this study the impact rates were determined by visual inspection and actual count of events whereas in the study of Gurnett et al. [1983] the rates were determined by listening for individual impacts on an audio recording of the waveforms. At the same six times, and for 5-min intervals centered at the

times of the wideband data recordings, we found the impact rates from the 16-channel spectrum analyzer data by counting the number of peaks that exceeded the amplitude threshold and correcting for the duty cycle and spacecraft interference, assuming that the impact rate does not change significantly over a period of few minutes.

Next, the corrected impact rates from the 16-channel spectrum analyzer data and from the wideband waveform data were compared. There is a difference between the former and the latter due to the different sensitivities of the two methods to dust impacts. The spectrum analyzer rates were lower than those determined using the waveforms since the wideband receiver is more sensitive to dust impacts than the spectrum analyzer. This increased sensitivity to dust impacts is because the distinctive nature of the impact waveform allows a very reliable count of even very small amplitude impacts. However, to assure that we are only using bursty events (dust impacts) in the spectrum analyzer data, we had to use quite large amplitude thresholds.

The difference between the impact rates derived by the two methods can be explained with the aid of Figure 7. This figure shows a hypothetical distribution of the number of impacts with impact "amplitude". The impact "amplitude" is a function of dust mass, dust and target composition, relative speed and impact geometry. If the PWS instrument was able to detect all possible particles then the number of impacts would be given by the entire area under the curve in Figure 7. However, the waveform receiver subsystem detects only impacts above its threshold as indicated by the hatched area labeled wideband data in the figure. Since the spectrum analyzer method has a lower sensitivity, hence, higher threshold as described above, then this method detects an even smaller fraction of the total distribution (labeled spectrum analyzer data in Figure 7). Therefore, for a reasonably regular distribution function, the

difference between impact rates from the two methods should be the difference in the areas of the two hatched regions in Figure 7. This provides the rationale for scaling the spectrum-analyzer rates described below. Hence, the next logical step was to calculate the average correction factor between the impact rates determined by the two methods. This way, the impact rates derived from the wideband waveform data can be used to calibrate the spectrum analyzer rates. The average correction factor was calculated to be 28.3 and the spectrum analyzer impact rates were multiplied by that factor. Figure 8 shows the agreement between the two impact rates after multiplying the rates derived from the spectrum analyzer by 28.3. Excluding the first and third points, one can see that the agreement between the rest of the points is quite good. The first and third point discrepancies were not included in the calculation of the average correction factor because of gaps in the spectrum analyzer data during the relevant time intervals.

A few comments are now appropriate about the response of the spectrum analyzer to short-duration signals since the time constant is a function of frequency. The response of the spectrum analyzer is subject to the constraint $\Delta f \Delta t \simeq 1$ where Δf is the filter bandwidth and Δt is the duration of the signal. As the channel frequency decreases Δf decreases and Δt increases since the bandwidth of the filters are $\sim \pm$ 15% of the center frequency of the channels. A signal sampled at, say 10 Hz, will take about one second to decay. Hence, this channel is effectively "active" for much longer than 50 msec and the duty cycle is greater than assumed above. At higher frequencies the filter bandwidth is larger (e.g., about 100 Hz for the 562-Hz channel) and the channel time constant is set by the 50-msec time constant of the log compressor. Therefore, at high frequencies, above about 500 Hz, short duration ($\sim$ 10 msec) pulses will be underestimated or missed completely, especially if they occur early in the 50-ms measurement period. Hence, the duty cycle in the 562 Hz channel is substantially less than

assumed above. This is one of the main reasons that in the lowest 4 channels of Figure 6 a large number of bursts were detected that exceeded the preset threshold and that substantially fewer bursts exceed the preset threshold in the upper 4 channels of Figure 6. By calibrating the spectrum analyzer impact rates with the waveform receiver impact rates (in essence Figure 8) we compensate for any errors that the varying time constant might have introduced.

The average ratio of impact rates determined by dividing the wideband waveform receiver data by the 16-channel spectrum analyzer data was used to multiply the impact rates from the 16-channel spectrum analyzer pertaining to the time from 0400 to 0425 SCET around the equatorial plane crossing of the spacecraft. The results are shown in Figure 9. A well defined peak can be seen when the spacecraft was about 2500 km below the equatorial plane. If one assumes that the particle distribution depends only on the distance z from the equatorial plane a Gaussian profile can be used in order to fit the impact rate profile. A good fit is given by a function of the form

$$R = R_0 + R_1 \exp[\frac{-(z-h)^2}{\Delta z_1^2}] \qquad (4)$$

where h is the offset of the symmetry axis from the equatorial plane and Δz is the thickness of the Gaussian component. The best fit values are $R_0 = 5 \pm 1\ s^{-1}$, $R_1 = 76 \pm 9\ s^{-1}$, $h = -2473 \pm 152$ km, and $\Delta z_1 = 2065 \pm 224$ km. This fit is shown as a solid line in Figure 9. Having obtained the impact rate profile, it is easy to return to Equation (3) and derive the number density profile. The results can also be seen in Figure 9 (right scale). The peak number density is a little over 0.002 m^{-3}, and it occurs when the spacecraft is about 2500 km south of the equatorial plane.

5. ANTENNA VOLTAGES AND GRAIN MASSES

As was mentioned in the previous chapter the threshold intensity for detecting dust impacts was set at 7.07×10^{-4} V. The actual mass detection threshold for the wideband waveform receiver for detecting dust impacts is smaller than the above because the waveform receiver has a higher sensitivity, hence lower threshold, than the 16-channel spectrum analyzer, a fact that was also shown in Figure 7.

It is useful to find the equivalent mass detection threshold for the waveform receiver since the impact rate detected from the spectrum analyzer data was calibrated with impact rates derived from the wideband waveform receiver. This threshold can be used as a lower limit for the derivation of particle sizes. The V_{rms} voltage profile was calculated for a few minutes around 0326 SCET. The frame at 0326 SCET is the last time that wideband waveforms were recorded before Voyager 1 crossed the equatorial plane. The V_{rms} profile around this time is shown in Figure 10. The lowest V_{rms} value at 0326 SCET was considered to be the voltage that corresponds to the waveform receiver mass detection threshold, m* since any larger impacting particle would exceed this voltage threshold. The lowest rms voltage was found to be approximately 5×10^{-4} V and is shown by an arrow in Figure 10. Next, the following equation was used to calculate m*,

$$m* = \frac{\beta C_A}{\alpha k} V_{rms} . \qquad (5)$$

Equation (5) was first used by Gurnett et al. [1983]. The constant β is instrument related and $\beta = 0.51$, C_A is the antenna capacity and $C_A = 90$ pF [Gurnett et al., 1983], k = 2.05 C/g and $\alpha = 0.0078$ [Tsintikidis et al., 1993]. Hence, m* was found to be 1.41×10^{-12} g which corresponds to a particle of 0.70 μm. In essence the Voyager 1 wideband waveform receiver would be able to detect particles that are about 0.7 microns in size or larger had it been used during the Voyager 1 equatorial crossing of Saturn. Since the spectrum analyzer rates were calibrated with the waveform data, this is also the effective size threshold for the spectrum analyzer-determined rates. Tsintikidis et al. [1993] used the following equation to calculate the rms mass of the particles that impacted the Voyager 2 spacecraft during the Saturnian ring plane crossing

$$m_{rms} = \frac{C_A}{\alpha\, k} \frac{1}{(R\tau)^{1/2}} V_{rms} \,. \qquad (6)$$

R is the impact rate and τ is the duration of a typical, unclipped pulse. Equation (6) will be used in the Voyager 1 case. As can be seen from the equation the V_{rms} value is required in order to calculate the masses.

The rms voltage for the PWS measurements is obtained by integrating over frequency the voltage spectrum that the instrument recorded during some time interval. Hence, each individual frequency (or channel) contributes to the total V_{rms}. The contribution is given by the ratio V_i/V_{rms}, where V_i is the voltage recorded by the ith channel. In general the V_{rms} voltage varies for different ring plane crossings. However, the contribution of each channel to the total rms voltage remains the same as long as the shape of the spectrum is the same. In other words, if V_{rms} is reduced V_i is also reduced in such a manner as to keep the aforementioned ratio

constant . The V_{rms}^{V2} recorded by Voyager 2 reached a maximum value of 0.137 V at the equator crossing. A typical peak voltage value, V_i, was obtained with the aid of Figure 11 for each of the lowest 4 channels (hence, i = 1 to 4) during the Voyager 2 equatorial crossing since the peaks were more pronounced in these channels. Also, because of the longer response of the narrowband filter , the instrument can more accurately measure the amplitude of short duration impulses. Next the ratios V_{rms}^{V2}/V_i were computed (see column 2 in Table 3). In essence the ratios show the inverse of the contribution to the total rms voltage profile from each frequency channel. Since the instrumentation and impact physics are identical it is expected that V_{rms}^{V1}/V_i ratio would be equal to the Voyager 2 V_{rms}^{V2}/V_i ratio. Hence, the following equality can be obtained:

$$\frac{V_{rms}^{V2}}{V_i^{V2}} = \frac{V_{rms}^{V1}}{V_i^{V1}}. \qquad (7)$$

The V_i^{V1} values can be taken to be the values of the bursts that exceeded the preset threshold indicated by the arrows in Figure 6. The only unknown in Equation (7) is V_{rms}^{V1}. Hence, solving Equation (7) for V_{rms}^{V1} a rough estimate of the rms voltage can be obtained in the Voyager 1 case. Four V_{rms}^{V1} values resulting from V_i^{V1} values for four typical bursts are shown in Table 3. The average voltage rms value is about 0.071 V. For this value the rms mass is 1.16×10^{-9} g by using Equation (6). The peak impact rate used in Equation (6) was R = 96 s^{-1} and the value τ = 1 msec was used for the duration of the pulse. Hence, the mass corresponds to a 6.5$-\mu$m dielectric particle with ρ = 1 g/cm^3 or to a 5.2$-\mu$m silicate with ρ = 2 g/cm^3.

The spikes in the spectrum analyzer data correspond to particles that are in the far right wing of the hypothetical distribution of Figure 7. If one considers the uncertainties pertaining to the geometry of the impact, or target material (e.g., gold has a yield constant that is six times larger than the yield constant of aluminum [Grün, 1981]), or the impact velocity then it is likely that the actual particle radii are less than 5 microns. Unfortunately there is no way for obtaining more precise results from the 16-channel spectrum analyzer data. It should be mentioned that the particle radii estimated for the Voyager 1 case with the above method are rough estimates.

One can use the above method to derive a V_{rms} profile using the first channel (10 Hz) for the Voyager 1 case. In the above discussion, we concentrated on the spikes in this profile. However, we concluded that the larger amplitudes may be due to effects other than large dust particles. Now we will analyze the background "continuum", assuming that it is at least partially due to dust impacts. The profile can be seen in Figure 12. This way we are more likely concentrating on the bulk of the particle distribution. Since we are interested in the background the large fluctuations can be ignored and a nominal value of 0.03 V can be used in Equation (6) which gives $m_{rms} = 5.34 \times 10^{-10}$ g. This value corresponds to a 5.0-μm dielectric particle or to a 4.0-μm silicate particle. It seems that the Voyager 1 spectrum analyzer is detecting particles that are up to a few microns in radius. The above value should be regarded as an upper limit because it is certain that plasma wave activity contributes to the total V_{rms}. Further, it was discussed that the time constant in the lowest channel is much larger than 50 milliseconds. Due to the long time constant and the fact that we have almost 16 impacts per second it is possible that some bursts may have resulted from a pile-up effect. Hence, the mass can also be seen as a cumulative mass of multiple impacts. Similar profiles to the one shown

in Figure 12 were obtained also for the second and third channels (17.8 and 31.1 Hz respectively).

6. DISCUSSION

A study has been performed of the impulsive noise that the PWS instrument detected near the equatorial plane during the Voyager 1 flyby of Saturn. It has been shown that this noise can be attributed in part to dust particle impacts. The mass threshold for detecting these particles is 1.41×10^{-12} g. The size of the particles is estimated to be a few microns. The particle impacts were detected when the spacecraft was in the vicinity of the equatorial plane and the impact rate peaked when the spacecraft was 2473 km south of the plane. The north-south thickness of the impact region is $2\Delta z = 4130$ km (full width half maximum value) based on a Gaussian fit. At the maximum impact rate, the maximum particle density was derived to be about 10^{-3} m^{-3}, which corresponds to interparticle distances on the order of 10 meters. The picture that emerges is of a 4000-km thick "disk" of micron sized particles located 2500 km south of the equatorial plane. The impact rates derived from the wideband receiver and the wings of Figure 7 indicate that there is also a broader region with lower dust densities or background "halo".

The properties of Saturnian dust particles have been studied before by Gurnett et al. [1983, 1987, 1991] and Tsintikidis et al. [1993] using the PWS instrument data. The difference between the method applied in this study and the method applied in the previous studies lies in how the impact rate profile and the mass values are derived. In the previous studies, the wideband waveform receiver (or high resolution) data frames were used to calculate impact rates. In this study, the 16-channel spectrum analyzer (or low resolution) data had to be used, since no high resolution data were available during the equator plane crossing. However, the

few high resolution data frames available at other times were still of use in order to calibrate the low resolution results. The current method could not have been used by, e.g., Gurnett et al. [1991] due to the uncertainty in the number of impacts responsible for each spike (see, for example, their Figure 2) since the very large impact rates lead to a high probability of multiple impacts within a 50-ms measurement interval. The same situation also occurs for the other planetary ring plane crossings by Voyager 2. It was fortunate that Voyager 1 crossed the E-ring region at a high speed and in a region of the ring with a relatively low density. The high relative speed between the particles and the spacecraft resulted in more charge being released during a dust impact ($k = 2.05$ C/g), hence, enabling the PWS instrument to detect the impact. The low number densities resulted in the spikes being well separated from each other. The above two factors allowed the spikes to be distinguished from the background plasma wave activity. Hence, we were able to derive the impact rate profile.

The particle masses in the present study were derived with the aid of the V_{rms} profile obtained during the Voyager 2 crossing of the Saturnian ring plane. In the present case the signal recorded by the PWS instrument is not attributed exclusively to dust impacts. Furthermore, if the response of the system is taken into account then the mass estimates should be regarded as an upper limit. The next step is to compare our findings with those of other studies.

It is useful to compare our findings with those of other studies. Showalter et al. [1991] performed an extensive analysis of a large set of the photometric data of Saturn's E-ring. They concluded that the ring consists of slightly nonspherical particles whose size distribution is narrow: 1.0 ($\pm$0.3) μm. This size is comparable to but smaller than the sizes obtained in this study. Randall [1993] concluded that the E-ring particle radii are in the range of 0.4 to 3.2 μm

which is in better agreement with our results. Randall [1993] derived these sizes by studying the absorption of energetic electrons in Saturn's magnetosphere.

One can use the best-fit Gaussian profiles or, equivalently, the number density profiles in order to derive the columnar number density perpendicular to the equator plane. The columnar number density is $\kappa = \pi(n_1 \Delta z_1)$ and $\kappa = 2.0 \times 10^4$ particles/m^2. The quantity n_1 is the number density that corresponds to R_1 of Equation (4). The quantity Δz_1 is the width of the Gaussian derived from Equation (4). The R_0 term has been ignored since it is smaller than R_1 and there is no way of calculating the thickness associated with it. From the columnar number density the optical depth can be derived. The optical depth, τ, is a measure of the fraction of the area covered by particles along the column perpendicular to the ecliptic plane. If a typical size of 4 μm is used, then the particle cross-sectional area is $A_0 = 5.02 \times 10^{-11}$ m^2. Hence, the optical depth becomes $\tau = A_0 \kappa = 1.04 \times 10^{-6}$, which is a rather small value. However, it should be kept in mind that the optical depth value is underestimated because it doesn't include particles below the instrument counting threshold. For the location traversed by Voyager 1 the optical depth normal to the equatorial plane as given by the photometric study of Showalter et al. [1991] is about 2.20×10^{-6}. The optical depth value calculated in the current study is very similar, smaller than the one calculated by Showalter et al. [1991] by a factor of 2. There are several reasons that can account for the difference. The Voyager 1 cameras detected all the particles that happened to be in their field of view (global technique), while the PWS instrument detected only the particles that were along the trajectory of the spacecraft and which were above a well defined sensitivity threshold (local technique). In other words the PWS instrument responded only (in essence) to the shaded area labeled spectrum analyzer data in Figure 7. The yield constant, k, comes from an empirical rule [Grün, 1981]. The k value for water is not

known so it had to be estimated from other materials. It could be off by a factor of 3 or more [Gurnett et al., 1983]. The impact geometry and site are not well known. Circular prograde motions are a good first order approximation. However, most of the particles are on moderately to very eccentric orbits [D. Hamilton, personal communication, 1992]. Eccentric orbits may introduce a 20% to 30% uncertainty in the relative velocity between the particles and the spacecraft and, hence, a comparable uncertainty in the impact rates (Equation 3). A smaller uncertainty (about 14 %) is introduced in the rms mass calculation since the rms mass varies inversely proportionally to the impact rate (Equation 6). Of course, it should be kept in mind that plasma wave activity is always masking some of the dust impact noise.

It is widely accepted that Enceladus is the primary source of the E-ring dust particles [Showalter et al., 1991; Horanyi et al., 1992; Hamilton, 1993]. According to Showalter et al. [1991] the E-ring originates mostly from geyser-like eruptions on the surface of Enceladus. The moon is located at 3.95 R_S and its surface is very smooth. The smoothness of the surface indicates that the moon is geologically active. Observations show that the thickness of the E-ring at its outer edge is about 40,000 km [Showalter et al., 1991]. The vertical structure of the E-ring, from computer simulations, favors a northward asymmetry rather than the southward asymmetry presented herein [D. Hamilton, personal communication, 1993]. The simulation preference is a result of the quadrupole component of the Saturnian magnetic field. Our results show that the dust is concentrated predominantly south of the equatorial plane. The vertical extent of the dust in the model used by Hamilton [1993] barely reaches the north part of the region derived from our study. On the other hand, the moon Tethys is located at about 4.89 R_S and lies closer (compared to Enceladus) to the location of the spacecraft ring plane crossing. It is possible that the particles detected by the PWS instrument may have originated from Tethys.

Our model accounts for the existence of dust up to about 2500 km north of the equatorial plane (right wing of the Gaussian profile in Figure 9). The fact that our technique does not detect dust that is predicted to exist more than a few thousand kilometers north of the equator plane [Horanyi et al. 1992; Hamilton 1993], has no obvious explanation.

A comparison of the PWS and PRA results is now appropriate. Aubier et al. [1983] attributed the noise that the Voyager 1 PRA instrument detected during the equator plane crossing to shot noise. Shot noise is due to electrons hitting the spacecraft antennas. The power spectrum of shot noise goes as f^{-2} and is a smooth, broadband spectrum [A. Keller, private communication, 1993]. However, the Voyager 1 PWS observations at Saturn did not have these characteristics. First, as it can be seen from Figure 6, the PWS noise exhibits bursts which are inconsistent with the smooth nature of the shot noise. Also, the power spectrum as derived from the PWS data during the equator crossing (see Figure 5) does not exhibit a clean f^{-2} behavior expected from shot noise.

ACKNOWLEDGEMENTS

The authors wish to acknowledge very stimulating discussions with Doug Hamilton and Larry Molnar. We wish to thank Larry Granroth and Scott Allendorf for the valuable advice they gave when it came to computer matters. Useful discussions with Andy Keller and Mihail Horanyi are also acknowledged. And last but not least Kathy Kurth for taking care of the appearance of the manuscript. This work was supported by contract 959193 with the Jet Propulsion Laboratory.

REFERENCES

Aubier, M. G., N. Meyer-Vernet, and B. M. Pedersen, Shot Noise from grain and particle impacts in Saturn's ring plane, Geophys. Res. Lett., 10, 5, 1983

Barbosa, D. D., and W. S. Kurth, On the generation of plasma waves in Saturn's inner magnetosphere, J. Geophys. Res., 98, 9351, 1992.

Bridge, H. S., J. W. Belcher, A. J. Lazarus, S. Olbert, J. D. Sullivan, F. Bagenal, P. R. Gazis, P. E. Hartle, K. W. Ogilvie, J. D. Scudder, E. C. Sittler, A. Eviatar, G. L. Siscoe, C. K. Goertz, V. M. Vasyliunas, Plasma observations near Saturn: initial results from Voyager 1, Science, 212, 217, 1981.

Burns, J. A., and L. Shaffer, Orbital evolution of circumplanetary dust by resonant charge variations, Nature, 337, 340, 1989.

Grün, E., Experimental studies of impact ionization, ESA Rep. (Paris), SP-155, 1981.

Gurnett, D. A., E. Grün, D. Gallagher, W. S. Kurth, and F. L. Scarf, Micron sized particles detected near Saturn by the Voyager plasma wave instrument, Icarus, 53, 236, 1983.

Gurnett, D. A., W. S. Kurth, F. L. Scarf, J. A. Burns, J. N. Cuzzi, and E. Grün, Micron-sized particles detected near Uranus by the Voyager plasma wave instrument, J. Geophys. Res., 92, 14,959, 1987.

Gurnett, D. A., W. S. Kurth, L. J. Granroth, S. C. Allendorf, and R. L. Poynter, Micron-sized particles detected near Neptune by the Voyager plasma wave instrument, J. Geophys. Res., 96, 19,177, 1991.

Hamilton, D. P., Motion of dust in a planetary magnetosphere: orbit-averaged equations for oblateness, electromagnetic, and radiation forces with application to Saturn's E ring, Icarus, 101, 244, 1993.

Horanyi, M., J. A. Burns, and D. P. Hamilton, The dynamics of the Saturn E ring particles, Icarus, 97, 248, 1992.

Humes, D. H., Results of Pioneer 10 and 11 meteoroid experiments: Interplanetary and near-Saturn, J. Geophys. Res., 85, 5841, 1980.

Kurth, W. S., D. A. Gurnett, and F. L. Scarf, A search for Saturn electrostatic discharges in the Voyager plasma wave data, Icarus, 53, 255, 1983.

Kurth, W. S. and D. A. Gurnett, Plasma waves in planetary magnetospheres, J. Geophys. Res., 96, 18977, 1991.

Meyer-Vernet, N., M. G. Aubier, and B. M. Pedersen, Voyager 2 at Uranus: Grain impacts in the ring plane, Geophys. Res. Lett., 13, 617, 1986.

Pedersen, B. M., N. Meyer-Vernet, M. G. Aubier, and P. Zarka, Dust distribution around Neptune: grain impacts near the ring plane measured by the Voyager planetary radio astronomy experiment, J. Geophys. Res., 96, 19187, 1991.

Randall, B. A., Energetic electrons in the magnetosphere of Saturn, to be submitted to J. Geophys. Res., 1993.

Scarf, F. L, and D. A. Gurnett, A plasma wave investigation for the Voyager mission, Space Sci. Rev., 21, 289, 1977.

Scarf, F. L, D. A. Gurnett, W. S. Kurth, and R. L. Poynter, Voyager 2 plasma wave observations at Saturn, Science, 215, 287, 1982.

Showalter, M. R., J. N. Cuzzi, and S. M. Larson, Structure and particle properties of Saturn's E ring, Icarus, 94, 451, 1991.

Tsintikidis, D., D. A. Gurnett, L. J. Granroth, S. C. Allendorf, and W. S. Kurth, Revised analysis of micron-sized particles near Saturn by the Voyager 2 plasma wave instrument, submitted to J. Geophys. Res., 1993.

Warwick, J. W., D. R. Evans, J. H. Romig, J. K. Alexander, M. D. Desch, M. L. Kaiser, M Aubier, Y. Leblanc, A. Lecacheux, and B. M. Pedersen, Planetary radio astronomy observations from Voyager 2 near Saturn, Science, 215, 582, 1982.

Xu, R.-L., and H. L. F. Houpis, The stability of the oscillation motion of charged grains in the Saturnian ring system, J. Geophys. Res., 90, 1375, 1985.

TABLE 1. The various impact rates (in s^{-1}) as derived from the 16-channel spectrum analyzer (SA) and the wideband waveform receiver (WFR) data at certain times (Day Of Year, DOY, and SpaceCraft Event Times, SCET) corrected for numerous effects.

DOY	SCET	SA Impact Rate	Impact Rate Corrected for Spacecraft Noise	WFR Impact Rate	Final Impact Rate
317	1001	0.09	0.01	5.36	0.28
317	1257	0.36	0.28	12.06	7.92
317	1830	0.17	0.09	13.57	2.55
317	2107	0.27	0.19	3.53	5.38
318	0109	0.43	0.35	5.72	9.91
318	0326	0.57	0.45	15.87	12.74

TABLE 2. Calculation of spurious event rates due to spacecraft thruster firings.

DOY	SCET	Duration (min)	Thruster activity rate (s^{-1})
316	0720	10	0.050
316	1850	15	0.110
316	2301	10	0.083
316	2335	15	0.067

TABLE 3. Calculation for the Voyager 1 V_{rms} values at the lowest 4 frequencies.

Frequency (Hz)	V_{rms}^{V2}/V_i^{V2}	V_i^{V1} (V)	V_{rms}^{V1} (V)
10.0	40.48	2.1×10^{-3}	0.085
17.8	39.96	1.0×10^{-3}	0.040
31.1	41.80	9.0×10^{-4}	0.038
56.2	29.92	4.0×10^{-3}	0.120

FIGURES

Figure 1: The trajectory of Voyager 1 plotted in a meridional plane passing through the spacecraft. The spacecraft crossed the equatorial plane at 6.24 R_S (1 R_S = 60,330 km). The radial extent of some of the rings is also shown. The circled A shows the position of the spacecraft when the last wideband data frame was taken before the equatorial plane crossing: 5.38 R_S radial distance and -4.53 degrees of latitude. The circled C.A. shows the closest approach position of the spacecraft: 3.05 R_S radial distance and -39.51 degrees of latitude.

Figure 2: The Voyager 1 plasma wave observations for 4 hours around the equatorial plane crossing. Note the low-frequency enhancement from about 0400 to 0430 SCET.

Figure 3: Frequency-time spectrogram for the Voyager 1 encounter with Saturn. SCET is shown in the abscissa along with the radial distance and latitude of the spacecraft. A gray-scale scheme is utilized where the highest intensities are shown in black and the lowest ones in white. Superimposed on the spectrogram is the profile of the electron cyclotron frequency $f_{ce} = 28|B|$, where f_{ce} is in units of Hz and B in units of nanoteslas. Also the lower hybrid resonance frequency f_{LH} profile can be seen, where $f_{LH} = \sqrt{f_{ce}f_{ci}}$, f_{ci} being the ion cyclotron frequency. The most intense feature is essentially a magnification (in time) of the feature tentatively labeled as dust in Plate 3 of Kurth and Gurnett [1991].

Figure 4: A series of broadband waveforms of the particle impact noise taken at 0326 SCET when the spacecraft was at radial distance of 5.38 R_S and latitude -4.53 degrees. The beginning of each impact is shown with an arrow.

Figure 5: The voltage spectrum during 0413 to 0414 SCET. The only condition satisfied for choosing this specific time was for the interval to belong to the feature of interest, in other words to the low-frequency equatorial enhancement of Figure 3. The bump at higher frequencies corresponds to the relatively narrowband feature above the electron cyclotron frequency (electron cyclotron harmonic emission). It can easily be seen that at frequencies above a few hundred Hertz the spectrum varies approximately as f^{-4}.

Figure 6: Voltages of the first 8 channels of the 16-channel spectrum analyzer near the equatorial plane. The position of the spacecraft is also shown at various SCET's. Note that the intensity decreases as the frequency increases. Also, note the bursty signals superimposed on a smooth background. The intensity threshold is indicated by an arrow for each channel.

Figure 7: A hypothetical distribution of the number of impacts with impact amplitude. Impact amplitude denotes the intensity of the signal and it depends on the particle mass, composition, speed, and impact geometry.

Figure 8: A comparison of the impact rates as deduced from the wideband data and the 16-channel spectrum analyzer data. The latter has already been multiplied by the average discrepancy factor of 28.3. The error bars are 1 σ.

Figure 9: The impact rate profile obtained from the 16-channel spectrum analyzer data. Note the clear peak centered at about 2500 km below the equatorial plane crossing by the spacecraft. The error bars are 1 σ.

Figure 10: The rms voltage profile obtained around 0326 SCET. At that time the last wideband data frame was taken. The arrow indicates the waveform receiver

voltage (5×10^{-4} V) that corresponds to a mass detection threshold of 1.41×10^{-12} g. This corresponds to a 0.7-μm particle.

Figure 11: This figure is adapted from Tsintikidis et al. [1993]. The time interval corresponds to the Voyager 2 crossing of the Saturnian ring plane and $V_{rms} = 0.137$ V.

Figure 12: The V_{rms} profile for Voyager 1 obtained with the aid of the V_{rms} profile of Voyager 2. The Voyager 1 profile was obtained for the first channel (10 Hz). Similar profiles in shapes and intensities were obtained for channels 2 and 3 (17.8 and 31.1 Hz respectively).

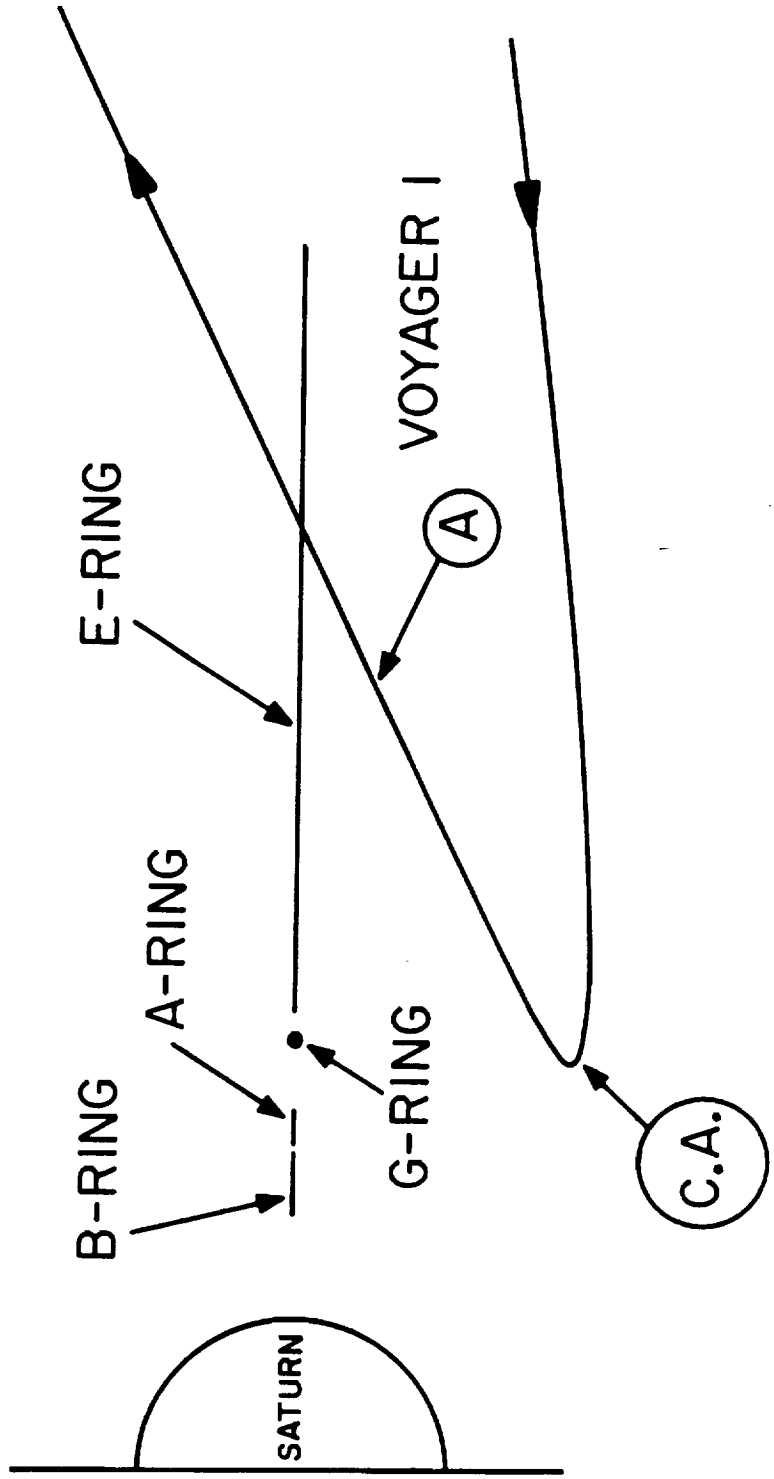

Figure 1

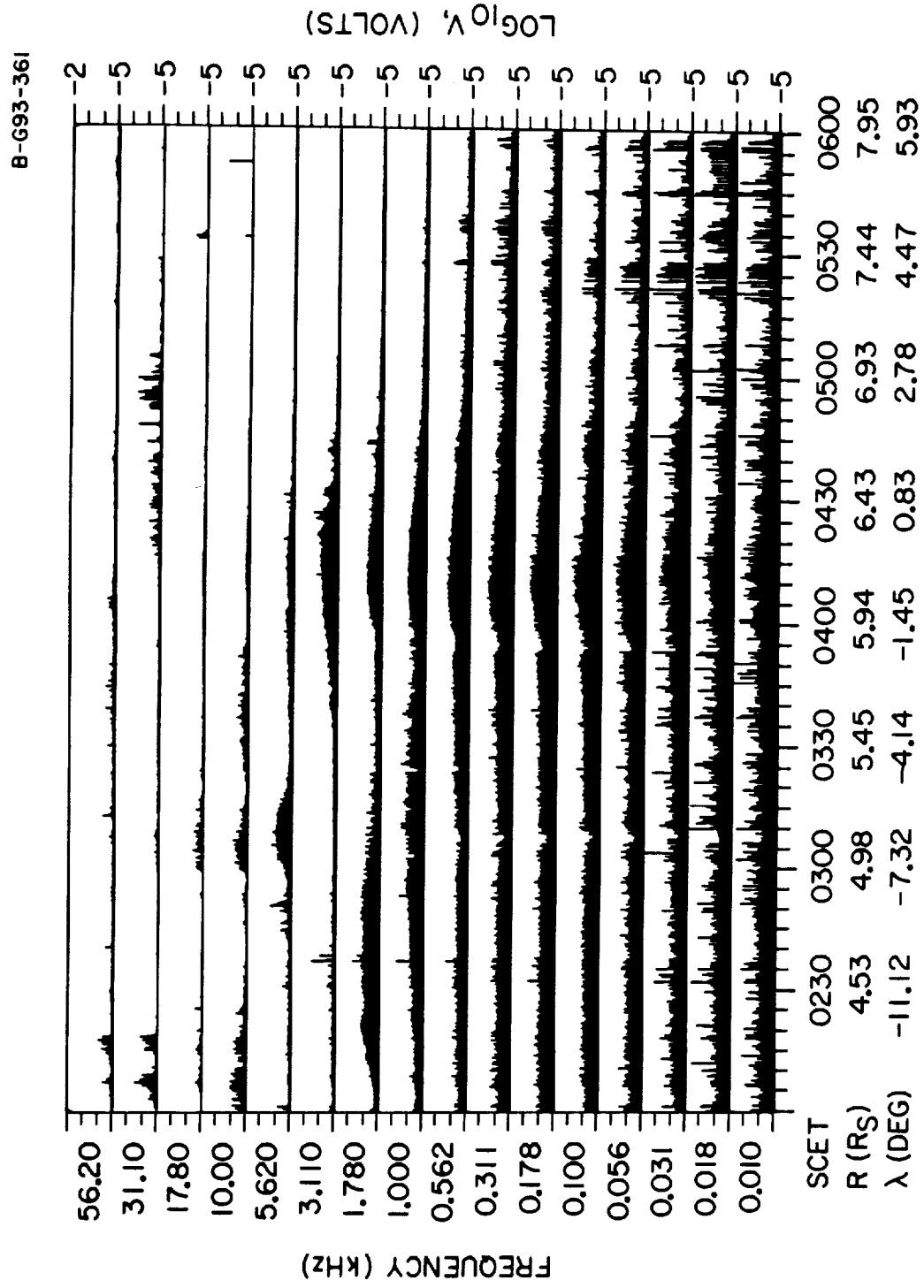
B-G93-361
LOG10 V, (VOLTS)
-2
-5
FREQUENCY (kHz)
56.20
31.10
17.80
10.00
5.620
3.110
1.780
1.000
0.562
0.311
0.178
0.100
0.056
0.031
0.018
0.010
SCET 0230 0300 0330 0400 0430 0500 0530 0600
R (RS) 4.53 4.98 5.45 5.94 6.43 6.93 7.44 7.95
λ (DEG) -11.12 -7.32 -4.14 -1.45 0.83 2.78 4.47 5.93
VOYAGER 1, NOVEMBER 13, DAY 318, 1980

Figure 2

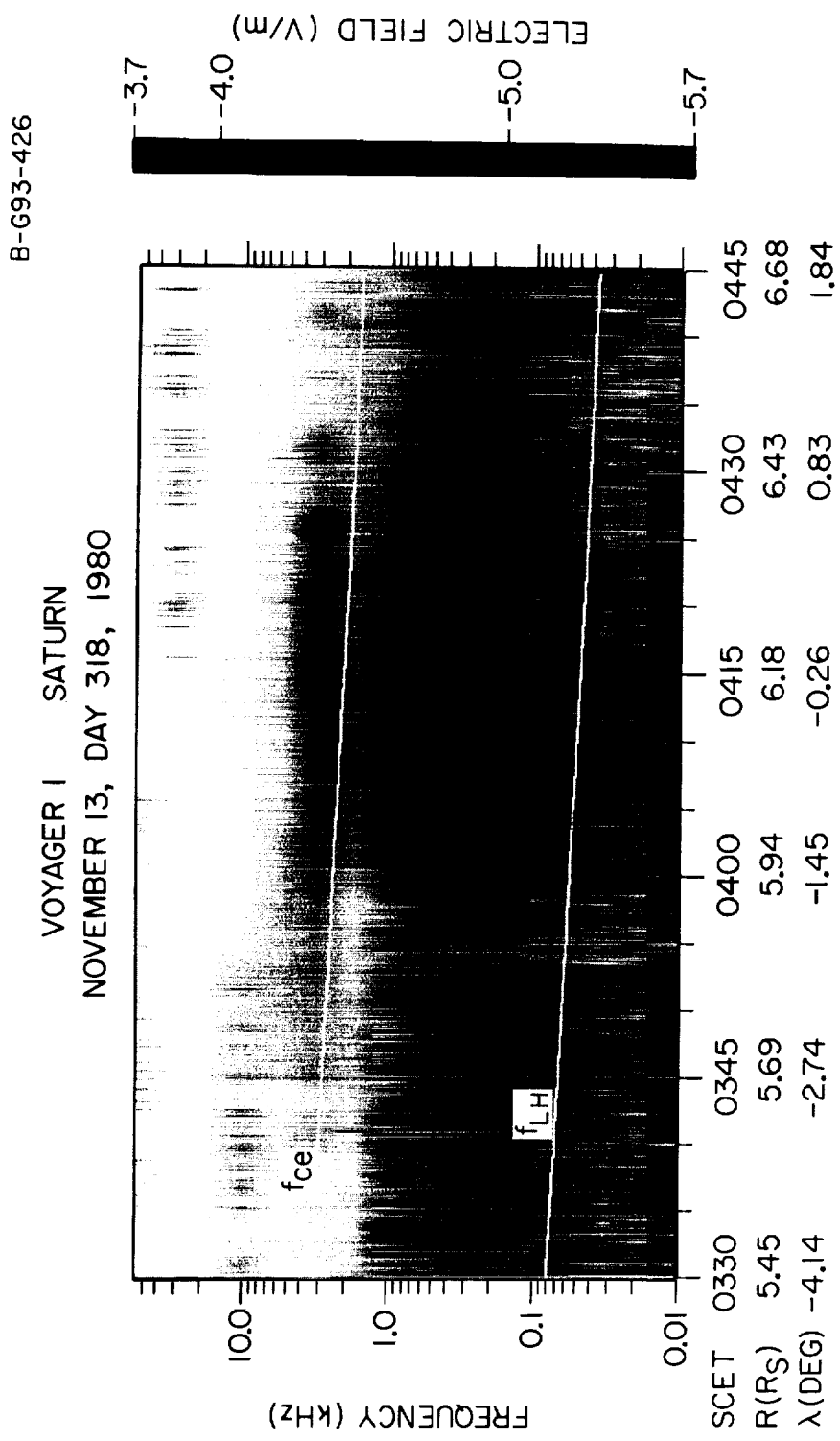
B-G93-426
VOYAGER I SATURN
NOVEMBER 13, DAY 318, 1980
ELECTRIC FIELD (V/m)
-3.7
-4.0
-5.0
-5.7
FREQUENCY (kHz)
10.0
1.0
0.1
0.01
f_{ce}
f_{LH}
SCET 0330 0345 0400 0415 0430 0445
R(R_S) 5.45 5.69 5.94 6.18 6.43 6.68
λ(DEG) -4.14 -2.74 -1.45 -0.26 0.83 1.84

Figure 3

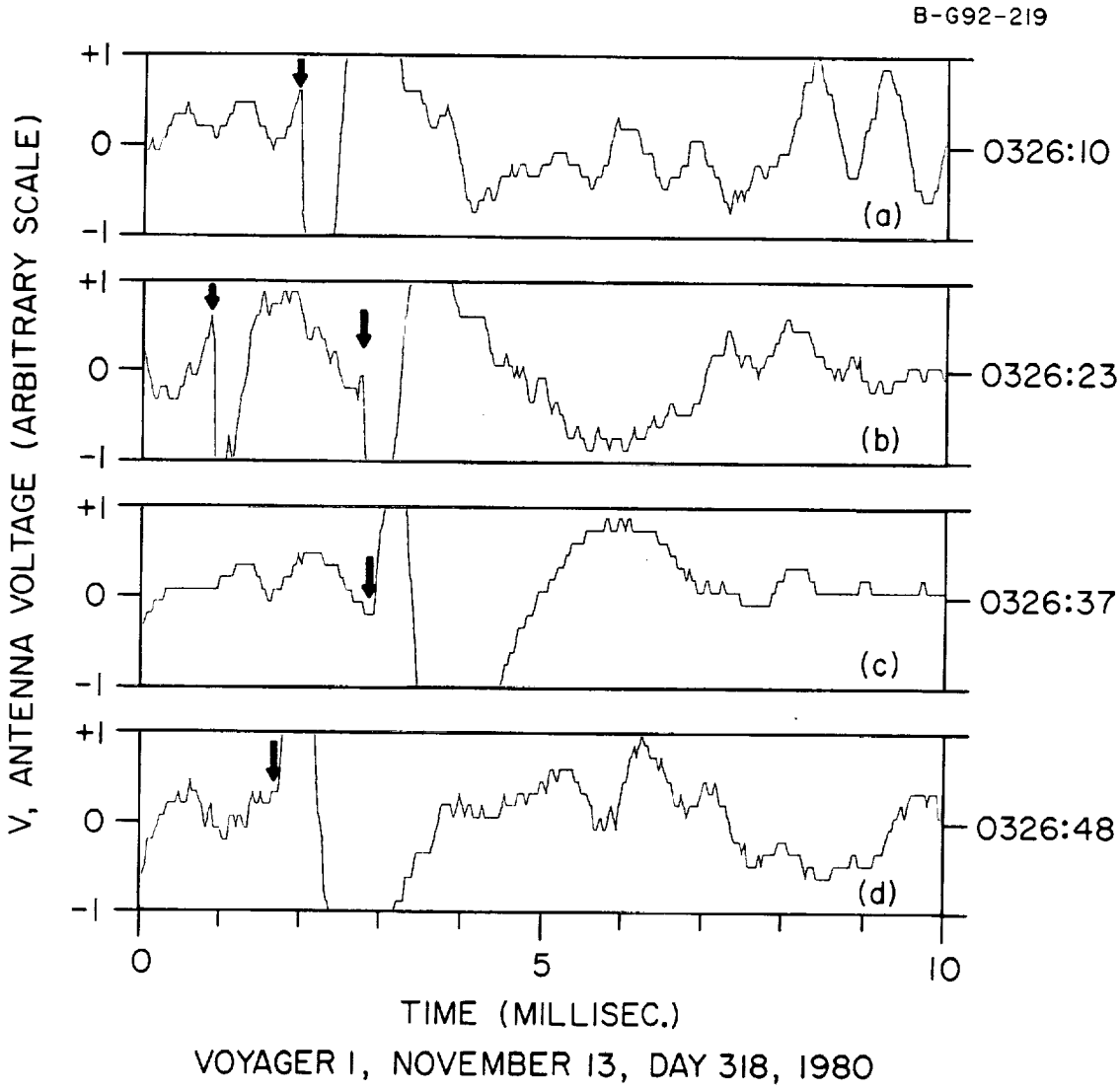
B-G92-219
V, ANTENNA VOLTAGE (ARBITRARY SCALE)
+1
0
-1
0326:10
(a)
0326:23
(b)
0326:37
(c)
0326:48
(d)
0
5
10
TIME (MILLISEC.)
VOYAGER 1, NOVEMBER 13, DAY 318, 1980

Figure 4

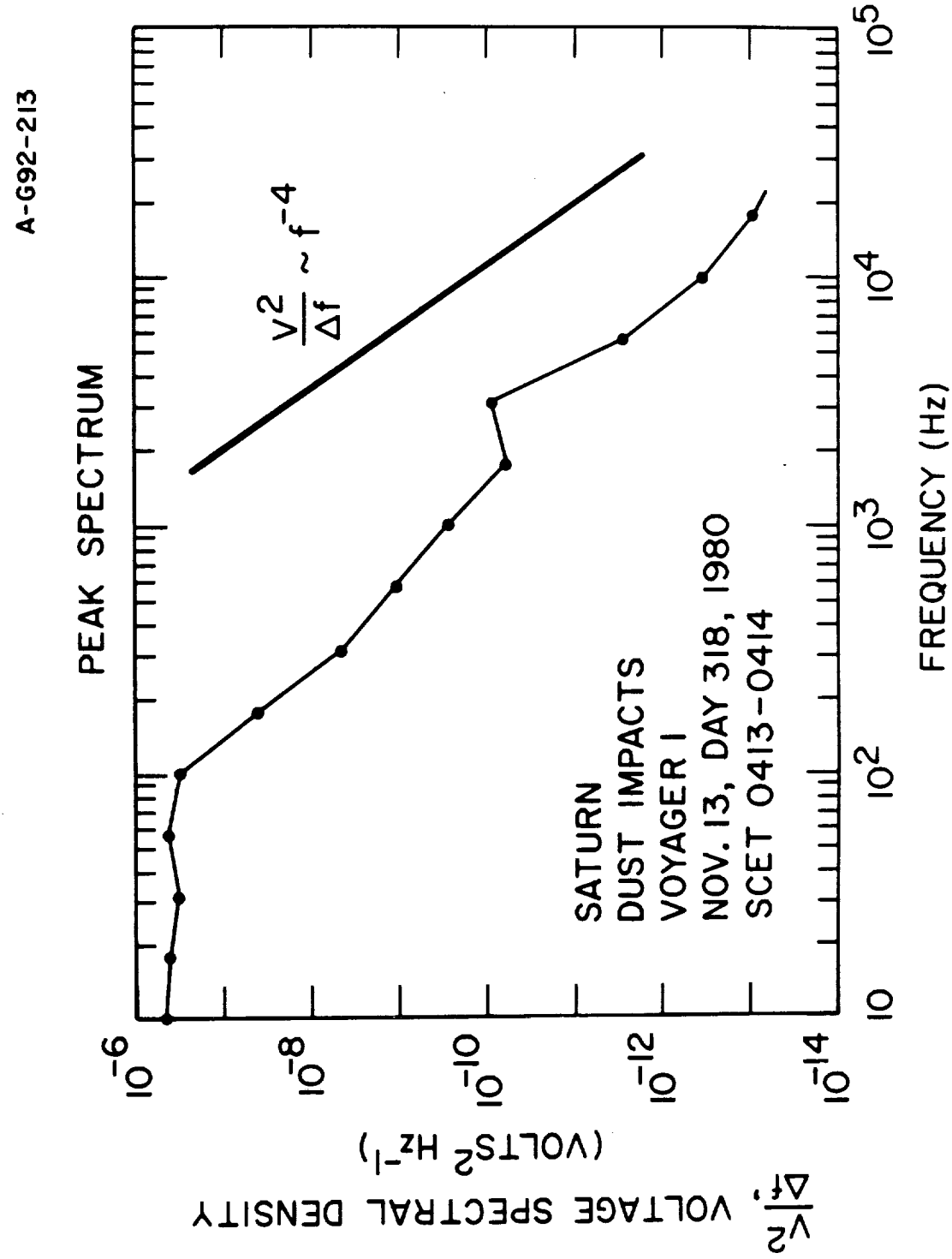
A-G92-213
PEAK SPECTRUM
$\frac{V^2}{\Delta f} \sim f^{-4}$
SATURN
DUST IMPACTS
VOYAGER 1
NOV. 13, DAY 318, 1980
SCET 0413-0414
$\frac{V^2}{\Delta f}$, VOLTAGE SPECTRAL DENSITY
(VOLTS^2 Hz^{-1})
10^{-6}
10^{-8}
10^{-10}
10^{-12}
10^{-14}
10
10^2
10^3
10^4
10^5
FREQUENCY (Hz)

Figure 5

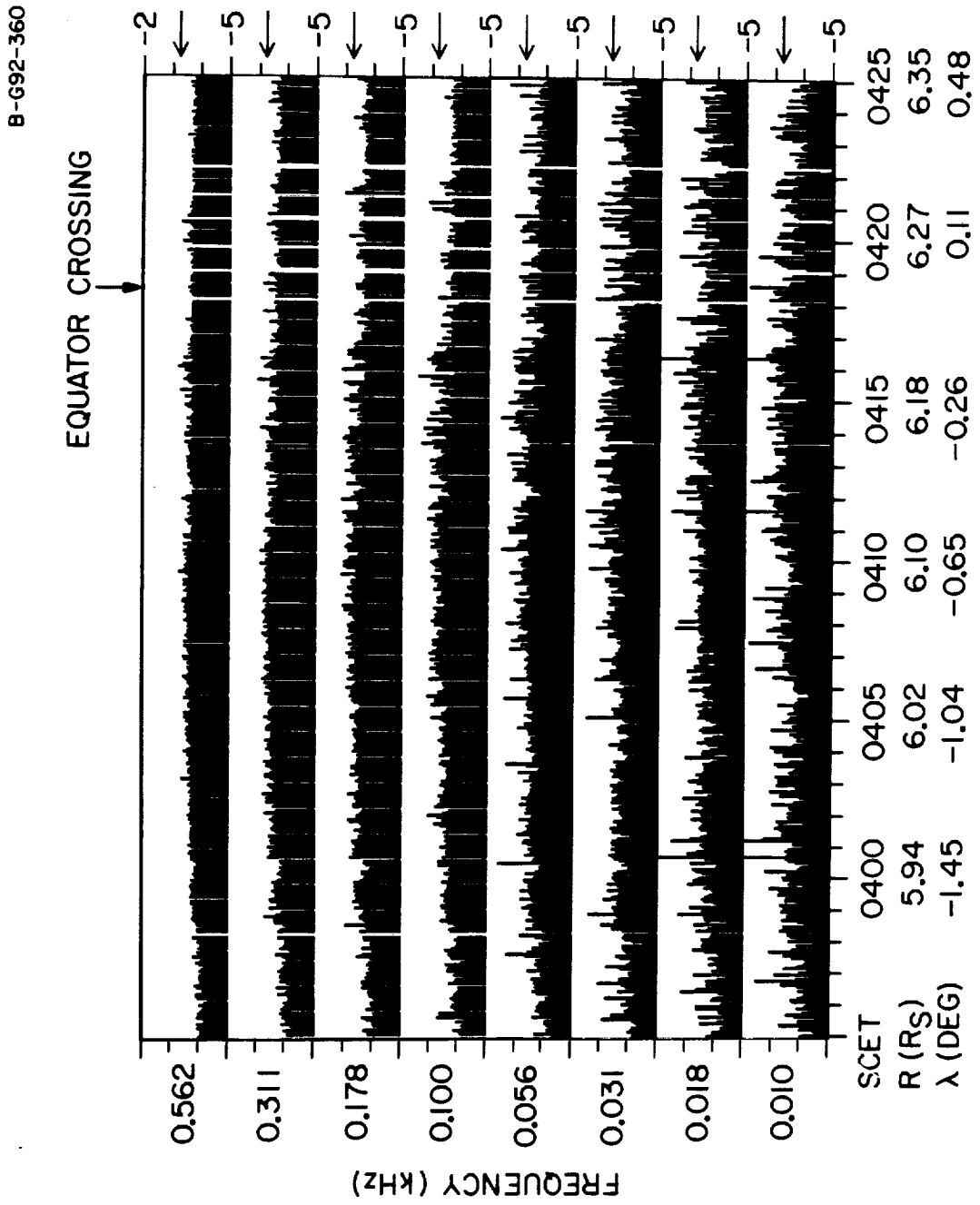
B-G92-360
EQUATOR CROSSING
LOG10 V, (VOLTS)
-2
-5
FREQUENCY (kHz)
0.562
0.311
0.178
0.100
0.056
0.031
0.018
0.010
SCET 0400 0405 0410 0415 0420 0425
R (RS) 5.94 6.02 6.10 6.18 6.27 6.35
λ (DEG) -1.45 -1.04 -0.65 -0.26 0.11 0.48
VOYAGER 1, NOVEMBER 13, DAY 318, 1980

Figure 6

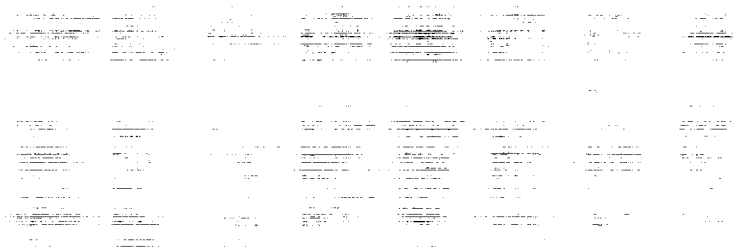

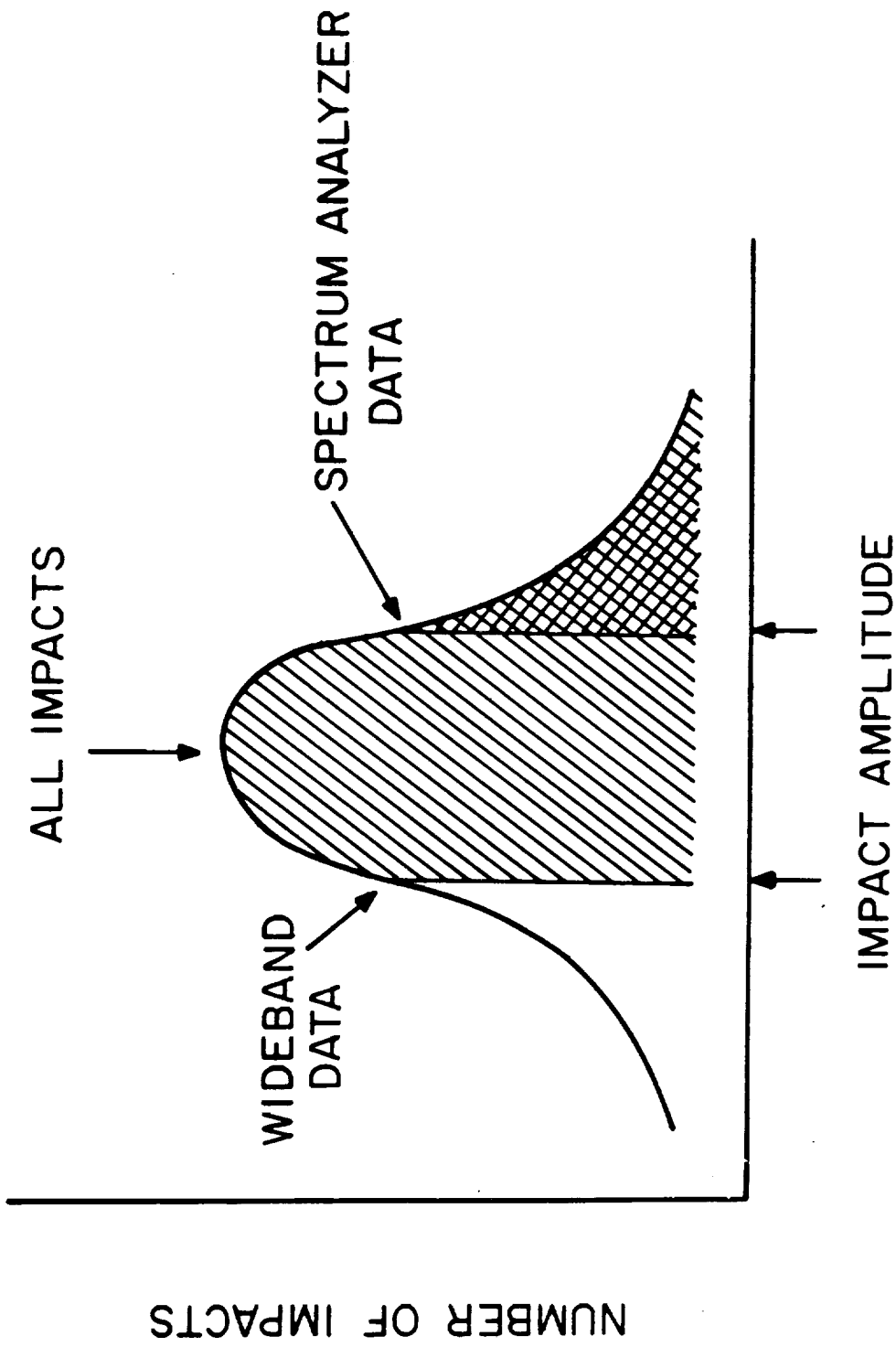
A-G93-351
NUMBER OF IMPACTS
IMPACT AMPLITUDE
ALL IMPACTS
SPECTRUM ANALYZER DATA
WIDEBAND DATA

Figure 7

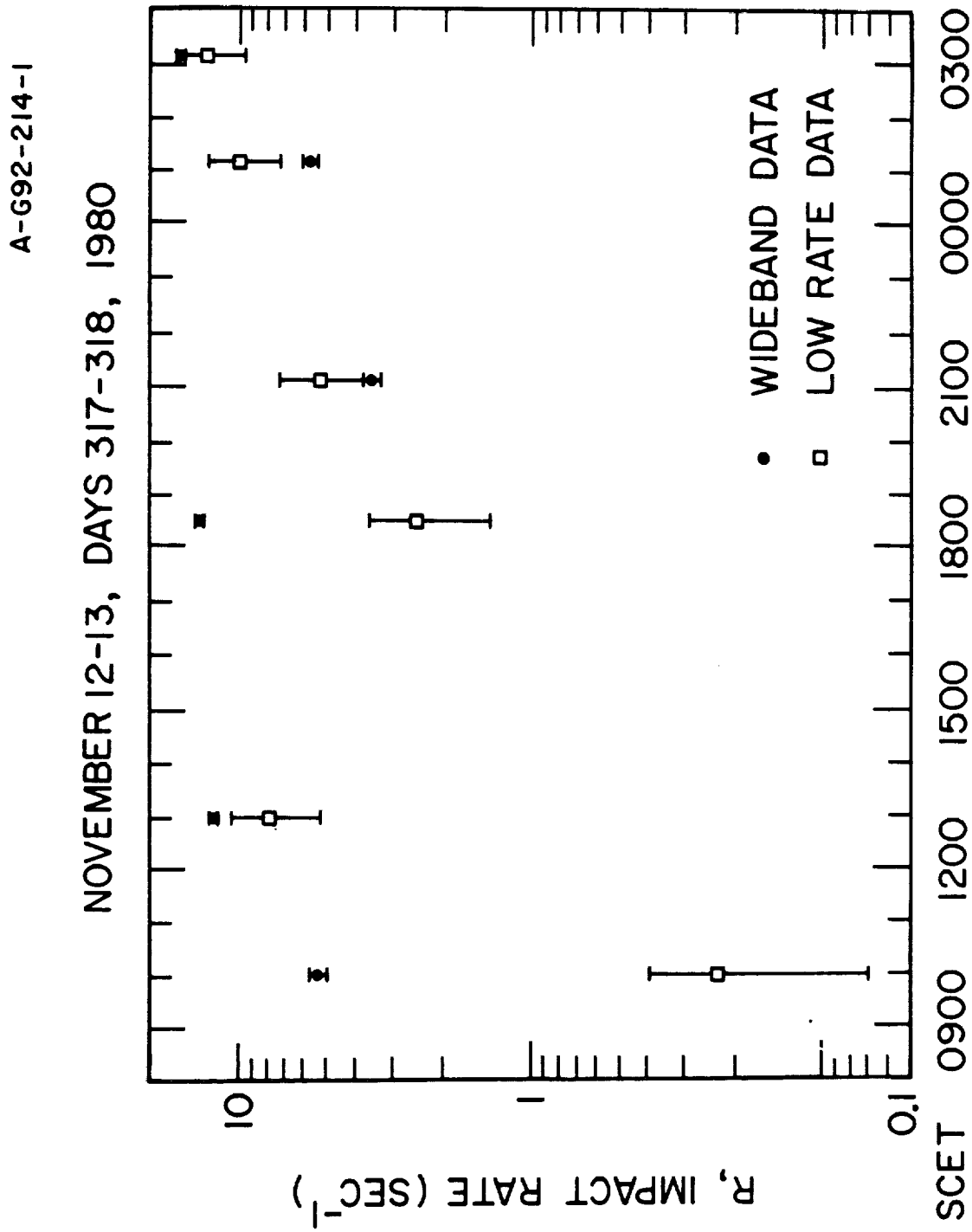
A-G92-214-1
NOVEMBER 12-13, DAYS 317-318, 1980
R, IMPACT RATE (SEC^{-1})
10
1
0.1
SCET 0900 1200 1500 1800 2100 0000 0300
WIDEBAND DATA
LOW RATE DATA

Figure 8

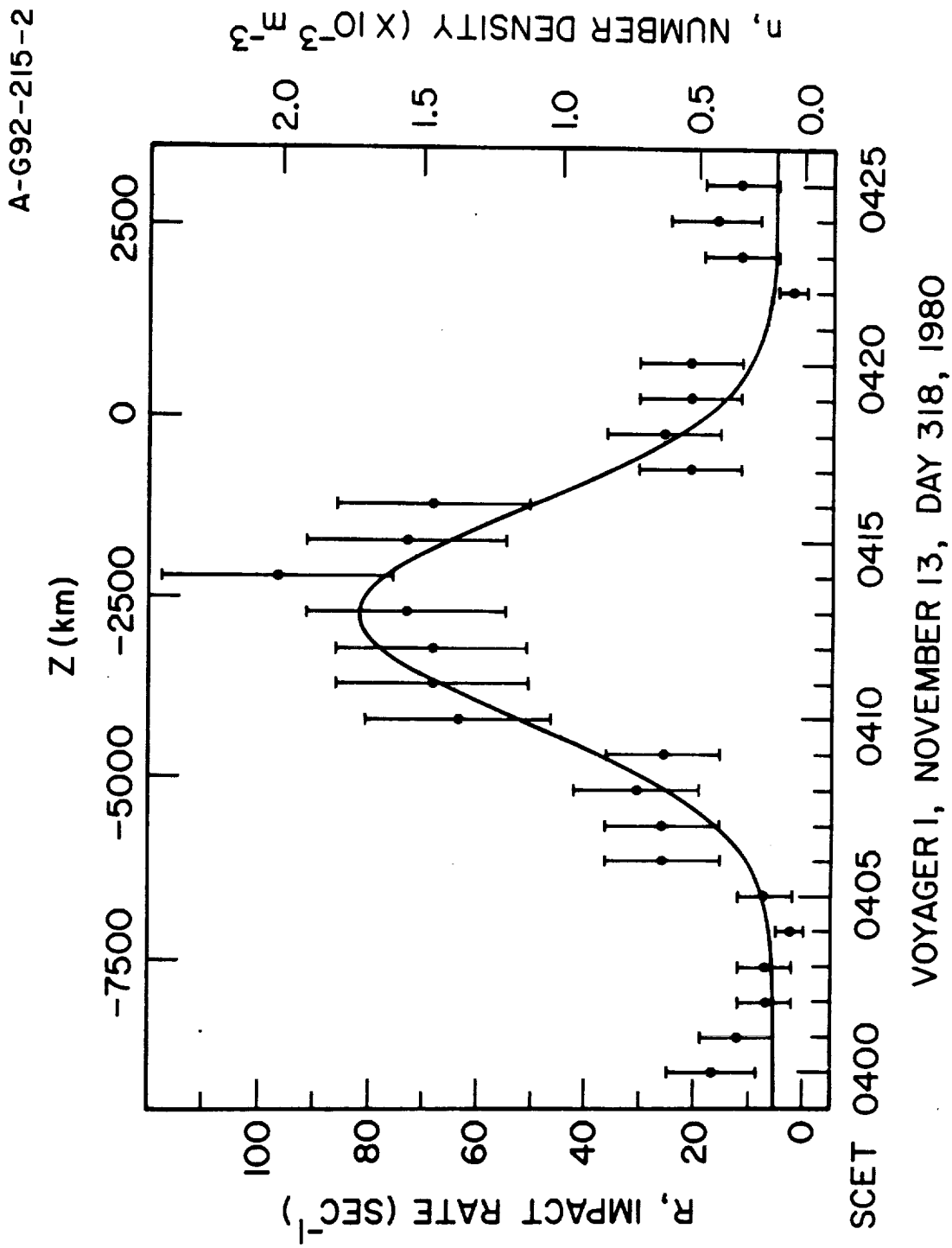
A-G92-215-2
n, NUMBER DENSITY (X 10⁻³ m⁻³)
2.0
1.5
1.0
0.5
0.0
Z (km)
2500
0
-2500
-5000
-7500
R, IMPACT RATE (SEC⁻¹)
100
80
60
40
20
0
SCET 0400
0405
0410
0415
0420
0425
VOYAGER I, NOVEMBER 13, DAY 318, 1980

Figure 9

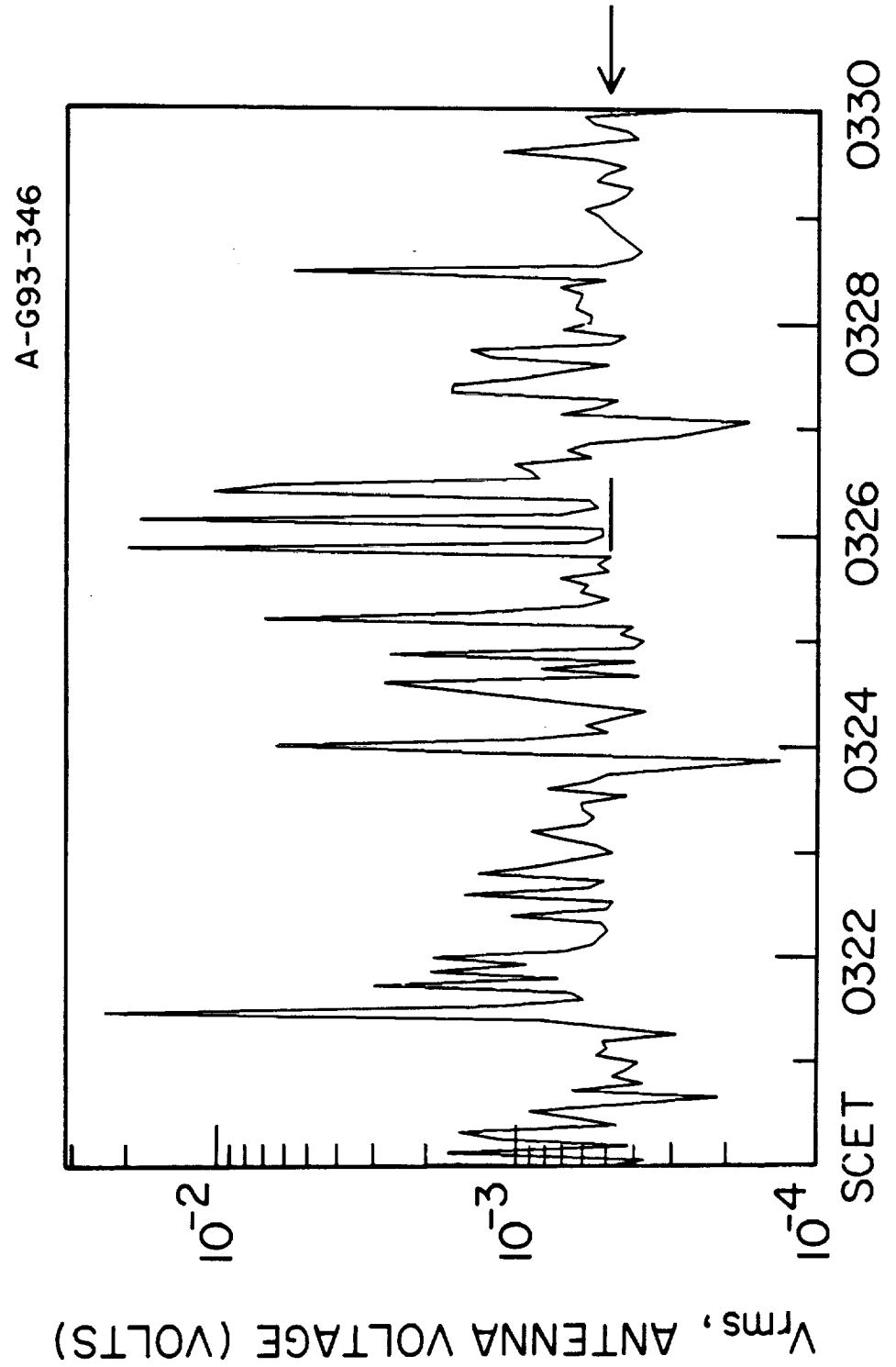
A-G93-346
V_{rms}, ANTENNA VOLTAGE (VOLTS)
10^{-2}
10^{-3}
10^{-4}
SCET 0322 0324 0326 0328 0330
VOYAGER 1, NOVEMBER 13, DOY 318, 1980

Figure 10

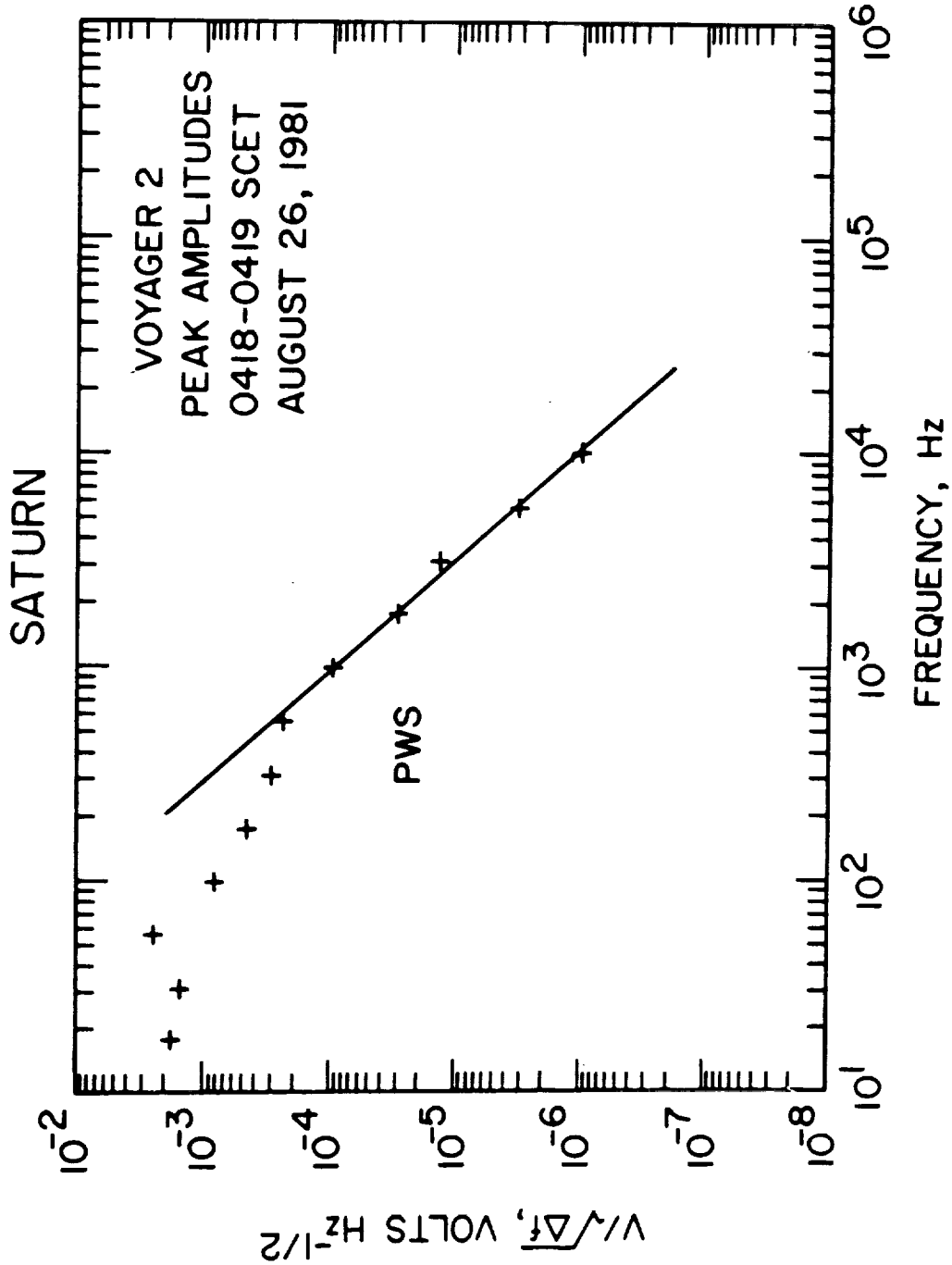
A-G93-350
SATURN
VOYAGER 2
PEAK AMPLITUDES
0418-0419 SCET
AUGUST 26, 1981
PWS
FREQUENCY, Hz
V/√Δf, VOLTS Hz^-1/2
10^-2
10^-3
10^-4
10^-5
10^-6
10^-7
10^-8
10^1
10^2
10^3
10^4
10^5
10^6

Figure 11

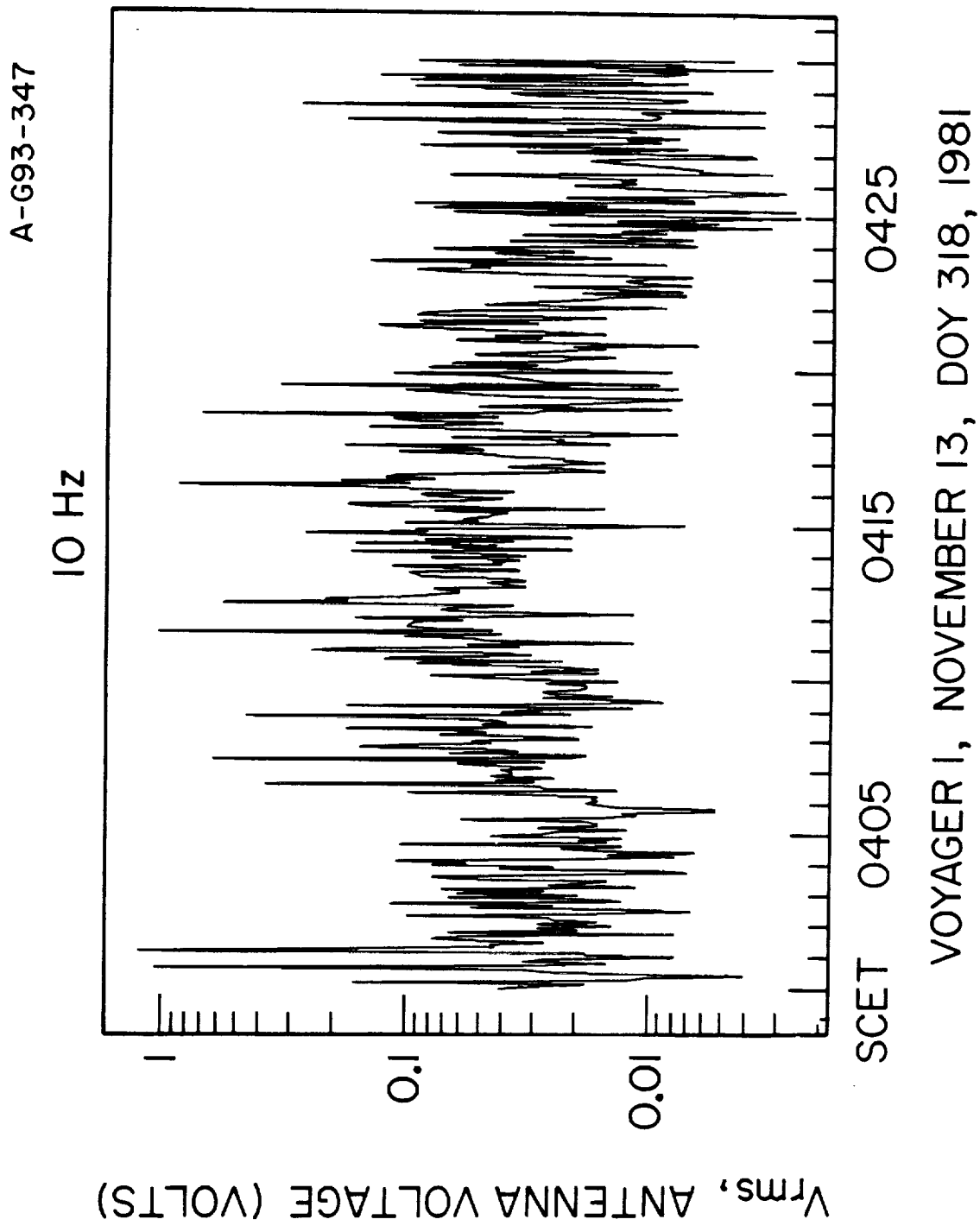
A-693-347
10 Hz
1
0.1
0.01
V_{rms}, ANTENNA VOLTAGE (VOLTS)
SCET 0405 0415 0425
VOYAGER 1, NOVEMBER 13, DOY 318, 1981

Figure 12